Advanced Correlations for Predicting Wax Precipitation in Crude Oil: A Study on Melting Point and Solid-State Transition Temperatures

Alfiya Khussainova
Kazakh-British Technical University, Tole bi str., 59, Almaty, 050000, Kazakhstan
a.khussainova@kbtu.kz (corresponding author)

Jamilyam Ismailova
Satbayev University, 22/5, Satbayev str., Almaty, 050000, Kazakhstan
j.ismailova@satbayev.university

Gulnaz Moldabayeva
Satbayev University, 22/5, Satbayev str., Almaty, 050000, Kazakhstan
g.moldabayeva@satbayev.university

Bakbergen Bekbau
KMG Engineering LLP, 8 Qonayev st., Astana, Z05H9E8, Kazakhstan
Bakbergen.Bekbau@gmail.com

Dinara Delikesheva
Satbayev University, 22/5, Satbayev str., Almaty, 050000, Kazakhstan
d.delikesheva@satbayev.university

Nargiz Zhumanbetova
Satbayev University, 22/5, Satbayev str., Almaty, 050000, Kazakhstan
n.zhumanbetova@satbayev.university

Abdulakhat Ismailov
Kazakh-British Technical University, Tole bi str., 59, Almaty, 050000, Kazakhstan
a.ismailov@kbtu.kz

Aigul Bakesheva
Satbayev University, 22/5, Satbayev str., Almaty, 050000, Kazakhstan
a.bakesheva@satbayev.university

Received: 18 November 2024 | Revised: 16 January 2025 and 27 January 2025 | Accepted: 30 January 2025

 DOI: https://doi.org/10.48084/etasr.9644

ABSTRACT

This study presents an in-depth investigation into the fusion properties, specifically the melting point and solid-state transition temperature, of crude oil samples from five distinct fields in Kazakhstan. These properties are critical for understanding and predicting wax precipitation, which poses significant challenges in the petroleum industry, particularly in cold climates where wax deposition can obstruct pipelines. Using advanced analytical techniques, including gas chromatography and pour point testing, new correlations were developed to more accurately predict these fusion properties for Kazakhstani crude oil. The proposed correlations outperform the existing models, offering closer alignment with the experimental data across a wide range of hydrocarbon compounds. The novelty of this research lies in its

tailored approach, which integrates experimental data, existing predictive models, and Python programming to develop a region-specific solution for Kazakhstani crude oil. By addressing the limitations of generalized models, the study highlights the importance of adapting predictive frameworks to specific oil compositions and regional conditions. These findings have substantial implications for the optimization of crude oil transportation and storage in cold environments, where wax deposition is a prevalent issue. The improved accuracy of the proposed correlations enables better predictability of wax-related flow assurance problems, contributing to more efficient and safer operations in the oil and gas industry. Furthermore, this work establishes a robust methodological framework that can be extended to other crude oil types and operational scenarios, paving the way for advancements in predictive modeling of wax precipitation under diverse environmental conditions.

Keywords-crude oil; wax precipitation; flow assurance; melting point; solid-state transition; correlation

I. INTRODUCTION

Crude oil remains a fundamental resource for energy production, with Kazakhstan serving as a significant contributor to the global oil supply. Efficient management of crude oil flow is essential to ensure the economic and operational viability of petroleum extraction and transportation, especially in cold climates. One of the most persistent challenges in this context is wax precipitation, which poses significant flow assurance issues. Wax deposition can obstruct pipelines, increase energy consumption, and heighten the risk of equipment failure, leading to costly delays and operational inefficiencies. Wax precipitation occurs when paraffins, heavy hydrocarbon components in crude oil, solidify under low-temperaturs. This issue is particularly acute in Kazakhstani oil fields due to the unique composition of crude oil in this region, characterized by high paraffin content. Existing predictive models and correlations often fall short of accurately forecasting wax precipitation in these specific conditions, as they fail to account for the distinct physicochemical properties of Kazakhstani crude oils.

Crude oil is a complex blend of various hydrocarbon and non-hydrocarbon components. Typically, the hydrocarbon components include asphaltenes, resins, aromatics, naphthenes, and paraffins. These components generally remain stable within the crude oil until a disturbance in the system's equilibrium occurs. Changes in pressure, temperature, or oil composition are primary factors that can disrupt this equilibrium, leading to instability in the crude oil system [1, 2]. In Kazakhstan, most crude oil contains heavy hydrocarbons that precipitate as paraffin (wax) solids at low temperatures. Paraffin is a heavy component of crude oil that solidifies below the pour point. The deposition of precipitated paraffin on pipeline walls presents a significant flow assurance challenge, as it reduces the cross-sectional area available for flow, potentially causing partial or complete blockage. Additionally, onshore facilities face increased energy consumption and higher risks of equipment failure due to paraffin blockages. Wax deposition also increases the viscosity of the oil mixture, which demands greater energy for crude oil transportation [3, 4]. Numerous methods have been developed both in academia and industry to predict, prevent, and mitigate the aforementioned flow assurance issues. Most of these methods focus on predicting the melting point and solid-state transition temperatures [5]. Currently, two main models are available for calculating wax deposition. The first assumes that the precipitated paraffin forms a solid solution, while the other assumes that the separated phase consists of multiple solid phases [6, 7]. Relevant studies involve statistical analyses and data preparation using field data from various oil fields. Melting point and solid-state transition temperatures were determined based on the results of these analyses.

In this study, we develop advanced correlations tailored to the specific properties of crude oil from five distinct fields in Kazakhstan. Using Python-based programming, we analyzed experimental data obtained through gas chromatography and pour point testing to create new models for predicting the melting point and solid-state transition temperatures. The proposed models offer improved accuracy compared to traditional approaches, providing a more reliable framework for anticipating wax precipitation and enhancing flow assurance strategies. By focusing on the specific characteristics of Kazakhstani crude oil, this research not only contributes to the existing body of knowledge but also offers practical solutions to one of the most pressing issues in petroleum engineering.

A. Melting Temperature

Authors in [3] presented a method for the thermodynamic prediction of vapor-liquid-solid paraffin phase equilibria in paraffinic hydrocarbon mixtures. The homogeneous solid solution S is assumed to be in equilibrium with a liquid solution L and a gas mixture G. In three-phase equilibrium, the fugacity of component i in the solid phase is equal to its fugacity in the liquid solution and gas mixture [3, 4]:

$$f_i^S = f_i^L = f_i^G \quad (1)$$

The equilibrium coefficient between solid phase and liquid solution is defined as:

$$K_i^{SL} = \frac{S_i}{X_i} = \left(\frac{\gamma_i^L}{\gamma_i^S}\right) \exp\left(\frac{\Delta H^f}{RT}\left(1 - \frac{T}{T^f}\right) + \frac{\Delta C_p}{R}\left(1 - \frac{T^f}{T} + ln\frac{T^f}{T}\right) + \int_o^P \frac{\Delta V}{RT} dP\right)_i \quad (2)$$

where γ is the activity coefficient, T^f is the melting temperature, ΔH^f is the melting enthalpy, ΔC_p is the change in heat capacity, ΔV is the change in melting volume, and X_i and S_i represent the mole fractions of the i^{th} component in liquid and solid phases, respectively [8].

The activity coefficients in (5) were calculated using a modified solution model:

$$\ln \gamma_i = \frac{v_i(\bar{\delta} - \delta_i)^2}{RT} \quad (3)$$

$$\bar{\delta_\iota} = \sum \phi_i \delta_i \quad (4)$$

$$\phi_i^L = \frac{X_i v_i}{\sum X_i v_i} \; ; \; \phi_i^S = \frac{s_i v_i}{\sum s_i v_i} \quad (5)$$

where v_i is the molar volume, δ_i is the mixing parameter, $\phi_i$is the fraction volume of the i^{th} component, and δ is the average mixability parameter.

The molar volume v_i in (7) can be estimated as:

$$d^L = 0.8155 + 0.6272 * 10^{-4} MW - \frac{13.06}{MW} \quad (6)$$

$$v = \frac{MW}{d^L} \quad (7)$$

where MW is the molar mass. To calculate the melting temperature (cloud point) and heat of fusion, the following formulas were proposed:

$$T_i^f = 374.5 + 0.02617 * MW_i - \frac{20172}{MW_i} \quad (8)$$

$$\Delta H_i^f = 0.1426 * MW_i * T_i^f \quad (9)$$

Authors in [8] studied a thermodynamic model for four phases involving vapor, liquid, wax-rich, and asphaltene-rich which was developed to predict the cloud and the amount of wax and asphaltene precipitation at different temperatures. They used Won's melting point temperature (T_i^f) correlation which depends on the value of molar mass (M_i):

$$T_i^f = 374.5 + 0.02617 M_i - \frac{20172}{M_i}, M_i \leq 450 \quad (10)$$

$$T_i^f = 411.4 - \frac{32326}{M_i}, \; M_i > 450 \quad (11)$$

The melting enthalpy (ΔH_i^f) is calculated without the weight function (($f(M_i)$)):

$$\Delta H_i^f = 0.5969 M_i T_i^f \quad (12)$$

The melting point temperature and melting enthalpy for naphthenic and aromatic carbohydrates were estimated by [9]:

$$T_i^f = 333.46 - 419.01 \exp(-0.008546 M_i) \quad (13)$$

$$\Delta H_i^f = 0.2208 M_i T_i^f \quad (14)$$

Heat capacity (ΔC_{Pi}) was determined by [10]:

$$\Delta C_{Pi} = 1.26957 M_i - 1.94014 * 10^{-3} M_i T \quad (15)$$

To evaluate the accuracy of the proposed method, the modeling results were validated by the experimental data of six samples from Nanyang Oil and North Sea Oil. With regard to North Sea Oil, the modeling results were compared with the results of [9, 11].

B. Solid-State Transition Temperature

Precipitated paraffin phase can exhibit retrograde phenomena like those in gas condensates. As a result of pressure reduction (at constant temperature), the amount of precipitated paraffin can at first increase, then decrease, and increase again. The model used in [6] takes into account as a correction term the Poynting and phase transitions in the solid state. Accounting for these effects confirms the suitability of the multisolid phase for calculations of wax deposition (onset and amount) [12, 13]. A new correlation was proposed in [6]:

$$T_i^{tr} = 366.39775 + 0.03609 M_i - 2.08796 \times \frac{10^4}{M_i} \quad (16)$$

Moreover, the authors proposed correlations for the enthalpies of melting and solid-phase transition of normal alkanes.

For M_i > 282 kg/kmol:

$$\Delta H_i^f = 0.1186 M_i T_i^f \quad (17)$$

$$\Delta H_i^{tr} = 0.0577 M_i T_i^{tr} \quad (18)$$

For M_i < 282kg/kmol:

$$\Delta H_i^t = 0.1777 M_i T_i^f \quad (19)$$

Authors in [14, 15] focus on low-temperature conditions in which the equilibrium between liquid-to-solid phase transition is poorly understood. They focused more on calculations of enthalpy-related phase transitions for components with different number of carbon atoms in the composition. For this reason, they proposed a co-crystal formation model of n-alkanes. The term co-crystal is explained as a nearly formed crystal with comparable size and compatible crystal structure. The model requires only the property values of the pure components.

For $20 \leq N_c \leq 36$:

$$\Delta H_{tr} = 6.7273 + \frac{24.4217}{1+\exp(7.2908 - 0.3350 N_c)} \quad (20)$$

For $9 \leq N_c \leq 35$:

$$\Delta H_{tr} = 22.9860 + \frac{18.9520}{1+\exp(6.6867 - 0.2623 N_c)} \quad (21)$$

The purpose was to develop a correlation for calculating Wax Appearance Temperature using a detailed hydrocarbon composition of crude oil. Different types of crude oil were studied and provided a good basis. DataFit software was used to develop the correlation, which allows several non-linear regressions [16-19]. The wax deposition point is considered not for a mixture but for a different range of components and a correlation was derived based on their content. The error from the initial data was less than 1%. As a result, two new correlations were proposed:

$$WAT = 6.808 X_1 + 0.366 X_2 + 3.381 X_3 + 3.028 X_4 \quad (22)$$

where X_1, X_2, X_3, and X_4 are the contents of components with the number of carbon atoms of: up to C_{10}, $C_{10\text{-}15}$, $C_{16\text{-}20}$, and $C_{21\text{-}30+}$, respectively.

$$WAT = 1.1017 X_1 + 0.075 X_2 + 1.611 X_3 + 213.586 \quad (23)$$

where X_1, X_2, and X_3 are the contents of components with the number of hydrocarbon atoms in the range of $C_{10\text{-}15}$, $C_{16\text{-}20}$, and $C_{21\text{-}30+}$, respectively.

The second correlation showed less error as a result of miscalculations. However, the disadvantage of these equations is that they cannot predict the phase equilibria at different temperature and pressure.

Table I shows a summary of the reviewed methods.

TABLE I. SUMMARY TABLE OF THE DIFFERENT MODELS AND APPROACHES FOR PREDICTING WAX PRECIPITATION

Model	Principles	Features	Disadvantages	Advantages
[3] (1986)	Assumes solid-liquid-vapor equilibrium. Uses thermodynamic equations for paraffin phase formation.	Incorporates molecular weight and heat of fusion. Used globally for wax prediction.	Fails to account for specific regional crude compositions.	Improved accuracy for Kazakhstani oil. Accounts for unique compositional characteristics.
[6] (2001)	Focuses on wax precipitation in gas condensate mixtures. Includes retrograde phenomena in solid phases.	Uses molecular weight and phase transitions. Applies multisolid phase models.	Designed for gas condensates. Less applicable for crude oil with high paraffin content.	Tailored specifically for paraffin-rich Kazakhstani crude oil. Better prediction in low-temperature scenarios.
[8] (2019)	Four-phase equilibrium model.	Comprehensive modeling of phase behavior under various conditions.	Relies heavily on detailed compositional data, not always available in field scenarios.	Simpler methodology. Easier application using linear and logarithmic regression with fewer input requirements.
[9] (1996)	Predictive model for melting temperatures based on hydrocarbon type and composition.	Emphasizes molecular weight and component properties.	Generalized for different crude oils. Lacks regional specificity.	Specifically calibrated to Kazakhstani oil properties. Reduced prediction errors for local fields.
Proposed	Developed using gas chromatography and pour point testing. Employs regression to derive new correlations.	Shares foundational principles with the models in [3, 6]. Relies on molecular weight and experimental data.	Incorporates experimental data tailored to Kazakhstani crude oil. Accounts for local paraffin compositions.	Superior accuracy for regional oils. Robust and adaptable to other fields with modifications.

II. MATERIALS AND METHODS

Gas chromatography separates and analyzes complex mixtures of substances. The process begins with an inert carrier gas, such as helium, passing through a chromatographic column filled with a stationary phase. The sample to be analyzed is introduced into the carrier gas stream, and as the mixture flows through the column, the components are separated based on their interactions with the stationary phase [20, 21]. The separated components exit the column and enter a detector, which converts the physical or chemical properties of each component into electrical signals. These signals are recorded and displayed as a chromatogram, allowing for the identification and quantification of the components. Gas chromatography is highly effective due to its ability to operate under precisely controlled conditions, such as temperature and pressure, which are maintained by thermostats and flow regulators. The equipment ensures high accuracy and sensitivity in detecting even minute quantities of substances [22, 23]. The Gas Chromatograph (Crystal 5000 Chromatek) was used for analyzing the compositional makeup of crude oil samples. The equipment separates and identifies hydrocarbon components based on their interaction with a stationary phase. Table II shows its characteristics and specifications. The chromatograph provides precise compositional data for hydrocarbons ranging from C_5 to C_{44}. This information is crucial for calculating fusion properties such as melting and solid-state transition temperatures.

The pour point tester (Table III) operates by methodically cooling a fluid sample to determine the lowest temperature at which it ceases to flow. The process begins by setting the desired test temperature on the touch screen display, which controls the cooling process. The sample is then prepared and, if necessary, heated to ensure it is in the appropriate state for testing. As the cooling progresses, the fluid's behavior is closely monitored, and the temperature is gradually lowered until the fluid no longer flows. During the test, the pour point tester records the precise temperature at which the fluid transitions from a free-flowing state to a semi-solid or solid state. This temperature is documented as the pour point, along with relevant test details such as sample identification, test conditions, and observations.

TABLE II. TECHNICAL CHARACTERISTICS OF THE CRYSTAL 5000 CHROMATEK CHROMATOGRAPH

Parameter	Value
Overall dimensions: width, depth, height (mm)	460, 590, 485
Electric power supply	AC 220V, 50 Hz
Power consumption (W)	peak -2500, average-700
Dimensions of the column installation area: width, depth, height (mm)	250, 169, 290
Inlet pressure of electronic flow and Pressure Regulators-PR (MPa)	from 0.36 to 0.44 (expandable to 1.25)
Number of Gas Flow Regulators (GFRs)	Up to 10
Carrier gas consumption (ml/min)	From 5 to 500
Number of detectors	Up to 3
Number of evaporators	Up to 3
Weight	38 kg
Operating temperature	Ambient +4 °C to 450 °C (or -100 °C to 450 °C with cryogenic cooling).
Detector type	Flame Ionization Detectors (FID) with a sampling frequency of 10–250 Hz.
Column specifications	Capillary column (10 m length, 0.53 mm diameter).
Thermostats	
Columns without a cryogenic cooling device	1 (Current +4 °C to 450 °C)
Columns with a cryogenic cooling device	1 (-100 °C to 450 °C)
Detectors	2 (up to 450 °C)
Vaporizers	2 (up to 450 °C)
Valves	2 (up to 250 °C)
Methane generators	1 (up to 450 °C)

TABLE III. POUR POINT TESTER CHARACTERISTICS

Name	Cloid Point Pour Point Tester by Trias Nathomi Chemindo
Temperature range	From room temperature to -45 °C
Refrigeration speed	70 °C/h
Refrigeration method	Refrigerated by compressor
Sensor	PT100 platinum resistance
Power	400-1000 W
Power supply	AC 220 V, 50 Hz

III. RESULTS AND DISCUSSION

A. Composition

The primary objective was to determine the composition of the provided oil samples. The chromatogram shows the response on the Y-axis and the yield time on the X-axis. A sharp increase in the response indicates that a component is released at the time of the peak. To determine which compound is being released, it is necessary to get acquainted with the standard. The standard and, consequently, the yield time of components for different equipment will be different, and depends on the type, model, and manufacturer of the gas chromatograph. Our equipment had installed a capillary column with a length of 10 m and a diameter 0.53 (Table III). This column has the name D2887, which indicates that the processing should take place according to the D2887 standard (Figure 1, Table IV). The standard is a guideline for conducting the experiment and indicates the yield time of various components if all the parameters of the experiment are set according to the standard. These parameters include temperature, carrier gas feed rate, carrier gas type, experiment time, etc. Since we know the yield time of the component according to the standard, the determination of the component composition becomes an easy task. This standard is able to show the presence of hydrocarbons with a number of carbon atoms from 5 to 44. The reason why this chromatograph cannot show the presence of hydrocarbons with less than 5 atoms is that these components have a low boiling point, less than room temperature, as a consequence of which they volatilize and their presence in oil samples is either very minimal or zero. The same principle is observed for non-hydrocarbon components found in oil, such as N_2, CO_2, H_2S, etc. These compounds also have a low boiling point, which is why they tend to volatilize, or in simple words change from liquid to gaseous state. Once a compound becomes a gas, it is difficult to detect and collect [7, 24].

TABLE IV. ASTM D2887 STANDARD

Chemical formula	Common name	Release time (min)
C_5H_{12}	Pentane	0.528
C_6H_{14}	Hexane	1.110
C_7H_{16}	Heptane	2.550
C_8H_{18}	Octane	4.774
C_9H_{20}	Nonane	6.379
$C_{10}H_{22}$	Decane	7.459
$C_{11}H_{24}$	Undecane	8.258
$C_{12}H_{26}$	Dodecane	8.935
$C_{14}H_{30}$	Tetradecane	10.079
$C_{15}H_{32}$	Pentadecane	10.590
$C_{16}H_{34}$	Hexadecane	11.082
$C_{17}H_{36}$	Heptadecane	11.523
$C_{18}H_{38}$	Octadecane	11.967
$C_{20}H_{42}$	Eicosane	12.752
$C_{24}H_{50}$	Tetracosane	14.153
$C_{26}H_{54}$	Hexacosane	14.768
$C_{30}H_{62}$	Triacontane	15.888
$C_{36}H_{74}$	Hexatriacontane	17.973
$C_{40}H_{82}$	Tetracontane	18.744
$C_{44}H_{90}$	Tetratetracontane	21.097

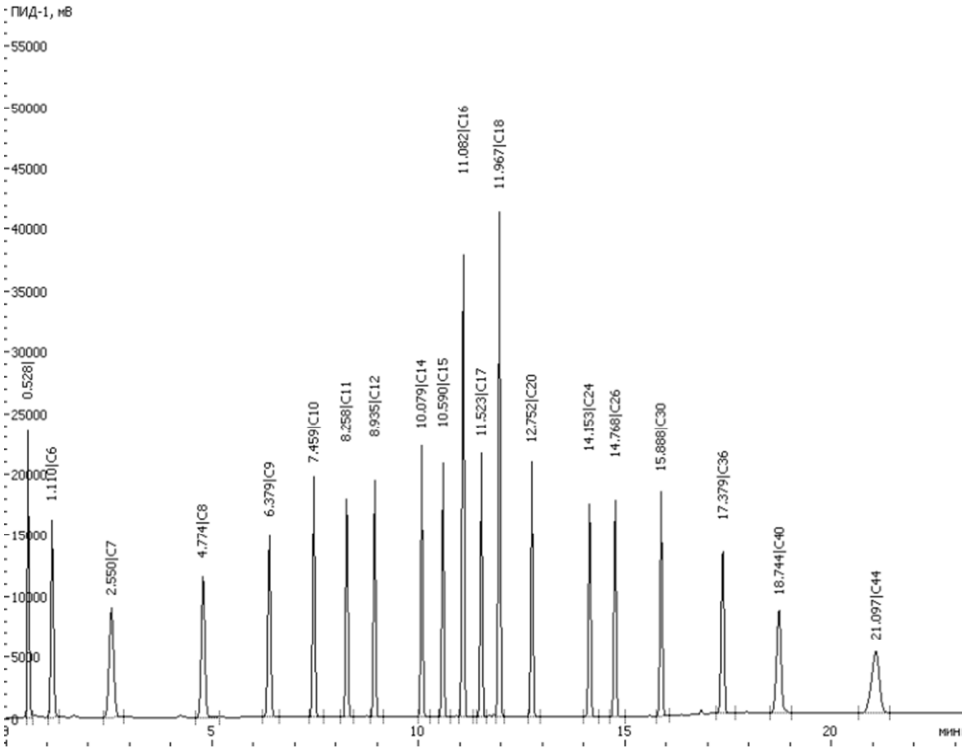

Fig. 1. The ASTM D2887 standard.

On the graph, we can see the response on the detector and the time indicating different changes in response. For example, a sharp increase in the response at times 10.500, 10.948, 11.376, 11.790, 12.179, etc. In order to determine which component gives the response it is necessary to compare the data with the standard (Table IV). According to the standard, at time 10.590, a hydrocarbon with 15 carbon atoms 15 - $C_{15}H_{32}$ is yielded. In our chromatogram, there is a peak with a time of 10.500 min. Since no significant peaks are observed in the close range to this time, we can conclude that this time signals the yield of the $C_{15}H_{32}$ component. The next peak is observed at time 10.948. The standard has an output of component $C_{16}H_{34}$ at time 11.082. Since the time deviation is small, again it can be concluded that 10.948 min corresponds to the yield of component $C_{16}H_{34}$. Thus, a detailed component composition was obtained for oil samples from different fields. To smooth out any errors and inaccuracies, each oil sample was run through the gas chromatograph 2-3 times. Then, the average values of the component content were taken [25]. We used oil samples from 5 fields in Kazakhstan where there is a problem with paraffin deposits and for the correctness of the data to improve the equation we conducted the experiments three times for each field. Thus, a detailed component composition was obtained for oil samples from different fields. When the list of possible compounds of the oil sample is obtained, the concentrations of these compounds are calculated. Many methods are available for calculating concentrations, but one of the simplest and least biased is the percentage normalization method. The method is based on the fact that different components will differ in peak area and peak height on a chromatogram depending on their content in the oil. The concentration of a compound is found by:

$$C_i = \frac{R_i}{\sum R} \quad (24)$$

where C_i is the concentration of compound i, R_i is the peak response (area or height), $\sum R$ is the sum of the responses of all the peaks in the chromatogram.

As an example, consider the results of the chromatogram for field A (Figure 2, Table V). In this case, the sum of all areas is 13115103.7. Knowing the area of each compound, we can find its concentration. For example:

$$C_{C_5H_{12}} = \frac{R_{C_5H_{12}}}{\sum R} = \frac{143251.845}{13115103.7} = 0.011 \text{ or } 1.1\% \quad (25)$$

The fluid compositions of the five oil samples are presented in Figures 2-16.

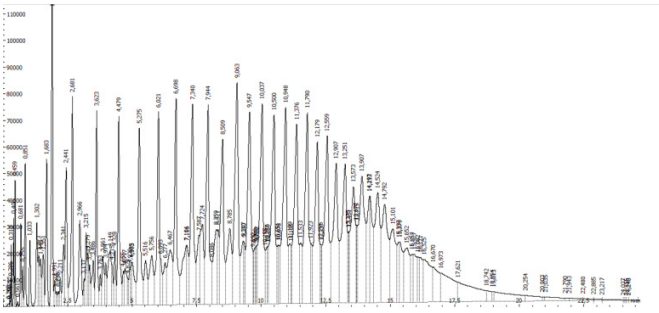

Fig. 2. Chromatogram from Field A, sample no. 1.

TABLE V. OIL COMPOSITION FOR FIELD A (SAMPLE 3)

Compound	MW, g/mol	Area	Concentration
C_5H_{12}	72.15	143251.845	0.011
C_6H_{14}	86.17	887670.925	0.068
C_7H_{16}	100.2	971729.246	0.074
C_8H_{18}	114.22	803974.842	0.061
C_9H_{20}	128.25	1044493.479	0.080
$C_{10}H_{22}$	142.28	565721.045	0.043
$C_{11}H_{24}$	156.3	495299.112	0.038
$C_{12}H_{26}$	170.33	608490.038	0.046
$C_{13}H_{28}$	184.35	512765.933	0.039
$C_{14}H_{30}$	198.38	489367.044	0.037
$C_{15}H_{32}$	212.41	918882.889	0.070
$C_{16}H_{34}$	226.43	447721.375	0.034
$C_{17}H_{36}$	240.46	501876.376	0.038
$C_{18}H_{38}$	254.48	466490.794	0.036
$C_{19}H_{40}$	268.51	470921.672	0.036
$C_{20}H_{42}$	282.54	340213.694	0.026
$C_{21}H_{44}$	296.56	337946.298	0.026
$C_{22}H_{46}$	310.59	297049.693	0.023
$C_{23}H_{48}$	324.61	438519.578	0.033
$C_{24}H_{50}$	338.64	304577.664	0.023
$C_{25}H_{52}$	352.67	447460.244	0.034
$C_{26}H_{54}$	366.69	456810.907	0.035
$C_{27}H_{56}$	380.72	234213.225	0.018
$C_{28}H_{58}$	394.74	73976.485	0.006
$C_{29}H_{60}$	408.77	497671.403	0.038
$C_{30}H_{62}$	422.8	232821.369	0.012
$C_{31}H_{64}$	436.82	153609.123	0.004
$C_{32}H_{66}$	450.85	55859.537	0.002
$C_{33}H_{68}$	464.87	32516.446	0.009

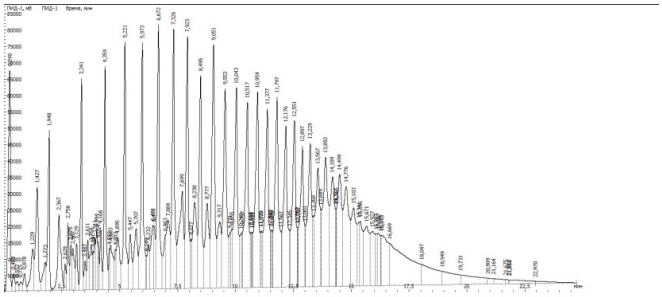

Fig. 3. Chromatogram from Field A, sample no. 2.

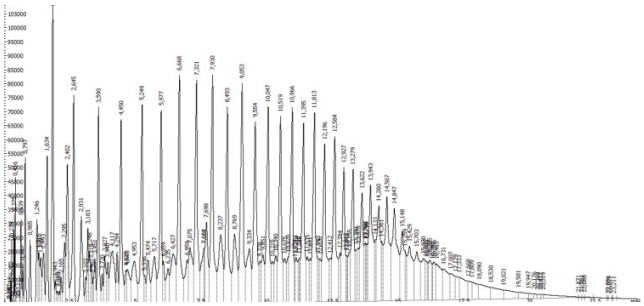

Fig. 4. Chromatogram from Field A, sample no. 3.

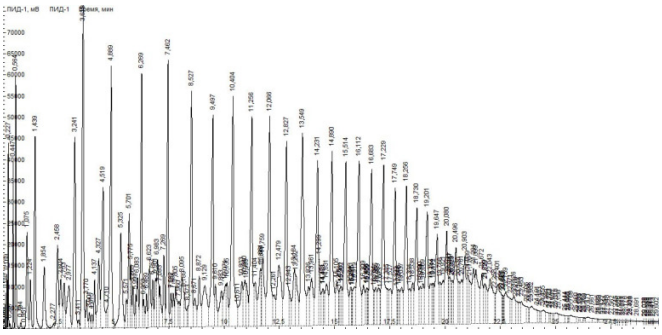

Fig. 5. Chromatogram from Field B, sample no. 1.

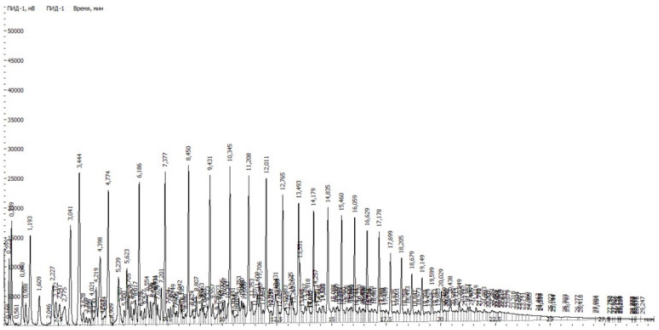

Fig. 6. Chromatogram from Field B, sample no. 2.

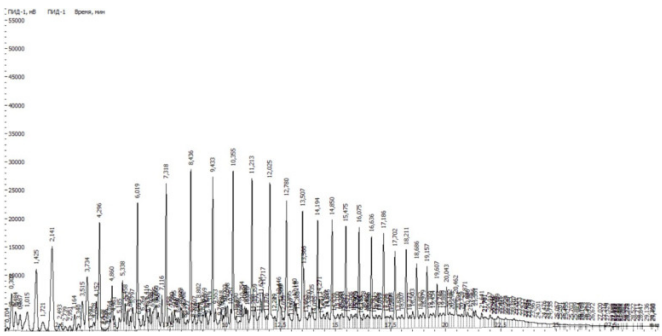

Fig. 7. Chromatogram from Field B, sample no. 3.

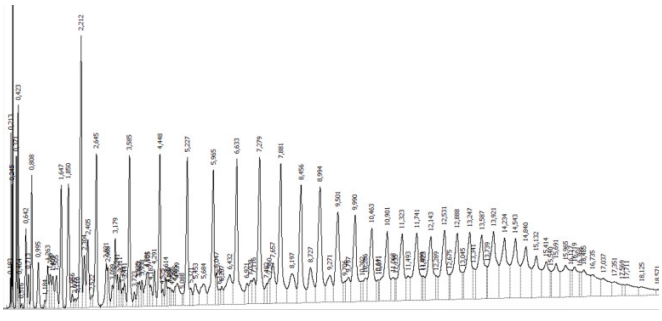

Fig. 8. Chromatogram from Field C, sample no. 1.

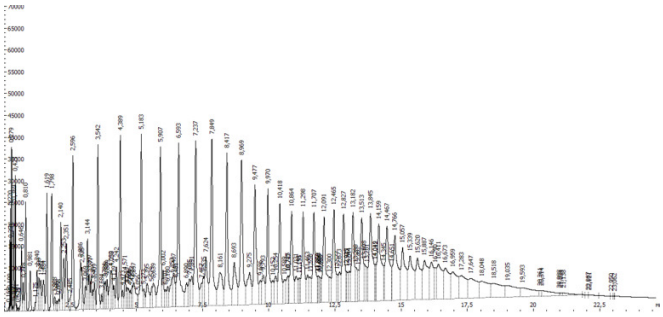

Fig. 9. Chromatogram from Field C, sample no. 2.

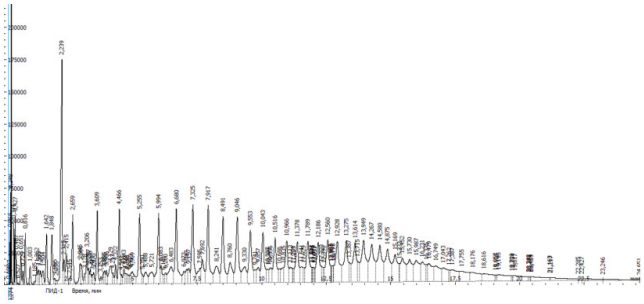

Fig. 10. Chromatogram from Field C, sample no. 3.

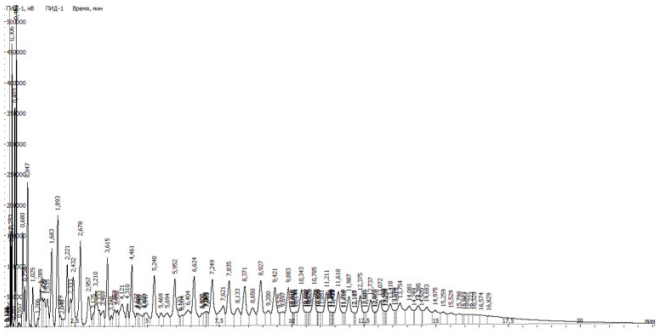

Fig. 11. Chromatogram from Field D, sample no. 1.

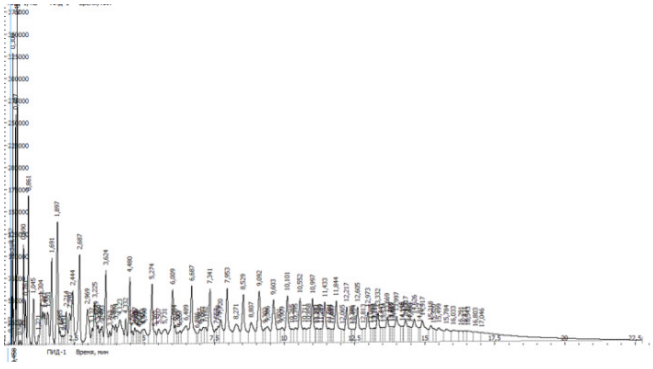

Fig. 12. Chromatogram from Field D, sample no. 2.

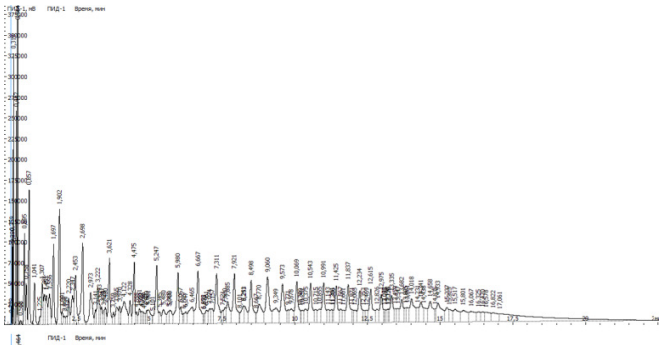

Fig. 13. Chromatogram from Field D, sample no. 3.

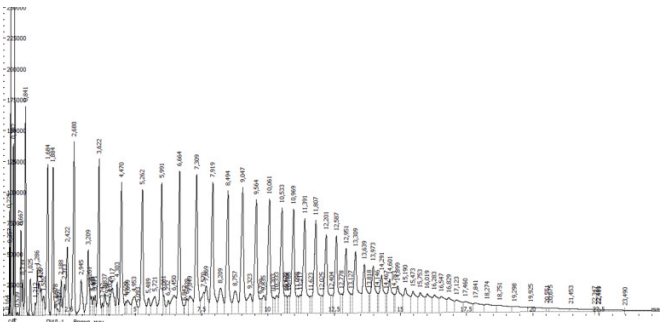

Fig. 14. Chromatogram from Field E, sample no. 1.

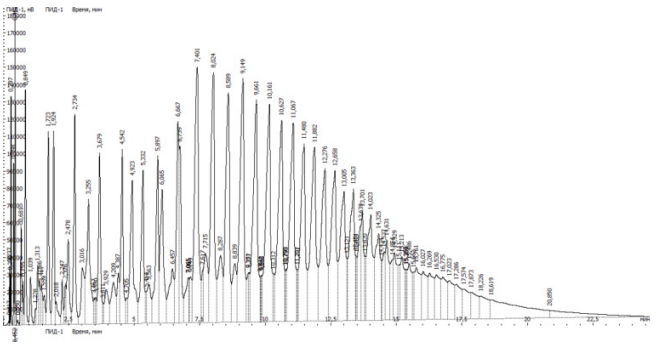

Fig. 15. Chromatogram from Field E, sample no. 2.

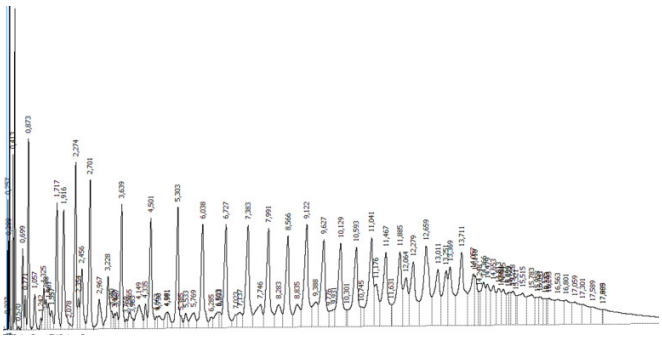

Fig. 16. Chromatogram from Field E, sample no. 3.

B. Molecular Weight and Fusion Property Calculations

Once the oil composition has been determined on the chromatograph, it is possible to calculate the molecular weight of the mixture using Kay's mixing rule. Most studies use molecular weight as the variable on which the melting point and solidus transition temperature depend. Kay's rule (1936) is [26]:

$$\theta = \sum_{i=1}^{N} z_i \theta_i \quad (26)$$

After the molecular weight is found, the melting point is calculated using Won's (1986) correlation:

$$T_i^f = 374.5 + 0.02617 * MW_i - \frac{20172}{MW_i} \quad (27)$$

The calculation of the solid-state transition temperature is done using the correlation of Nichita (2001):

$$T_i^{tr} = 366.39775 + 0.03609 M_i - 2.08796 \times \frac{10^4}{M_i} \quad (28)$$

By applying Kay's rule, the molecular weight for the mixture can be calculated:

$$\theta = \sum_{i=1}^{N} z_i \theta_i \quad (29)$$

$$MW = \sum_{i=1}^{N} z_i MW_i = 0.79 + 5.83 + 7.42 + \cdots + 4.11 = 218.43 \quad (30)$$

Knowing the molecular weight, it becomes possible to calculate the fusion properties using the equations of Won (1986) and Nichita (2001):

$$T_i^f = 374.5 + 0.02617 * MW_i - \frac{20172}{MW_i} = 374.5 + 0.02617 * 218.43 — \frac{20172}{218.43} = 287.86\ °K = 14.71\ °C \quad (31)$$

$$T_i^{tr} = 366.39775 + 0.03609 M_i - 2.08796 \times \frac{10^4}{M_i} = 366.39775 + +0.03609 * 218.43 - \frac{20879.6}{218.43} = 278.69\ °K = 5.54°C \quad (32)$$

This calculation was carried out for all 5 fields and, depending on the number of experiments, 2-3 times for each field. The results of the calculations are shown in the following Tables and Figures.

TABLE VI. FLUID COMPOSITION OF CRUDE OIL FROM FIELD A

Chemical formula	Molecular weight, g/mol	Avg. concentration, %
C_5H_{12}	72.15	0.624
C_6H_{14}	86.17	5.760
C_7H_{16}	100.2	6.152
C_8H_{18}	114.22	5.985
C_9H_{20}	128.25	7.305
$C_{10}H_{22}$	142.28	3.848
$C_{11}H_{24}$	156.3	3.444
$C_{12}H_{26}$	170.33	4.582
$C_{13}H_{28}$	184.35	5.306
$C_{14}H_{30}$	198.38	5.478
$C_{15}H_{32}$	212.41	5.129
$C_{16}H_{34}$	226.43	3.771
$C_{17}H_{36}$	240.46	4.176
$C_{18}H_{38}$	254.48	3.663
$C_{19}H_{40}$	268.51	2.360
$C_{20}H_{42}$	282.54	3.270
$C_{21}H_{44}$	296.56	3.297
$C_{22}H_{46}$	310.59	3.079
$C_{23}H_{48}$	324.61	4.839
$C_{24}H_{50}$	338.64	2.289
$C_{25}H_{52}$	352.67	3.266

$C_{26}H_{54}$	366.69	3.394
$C_{27}H_{56}$	380.72	2.195
$C_{28}H_{58}$	394.74	1.021
$C_{29}H_{60}$	408.77	1.829
$C_{30}H_{62}$	422.8	1.852
$C_{31}H_{64}$	436.82	0.484
$C_{32}H_{66}$	450.85	0.659
$C_{33}H_{68}$	464.87	0.943

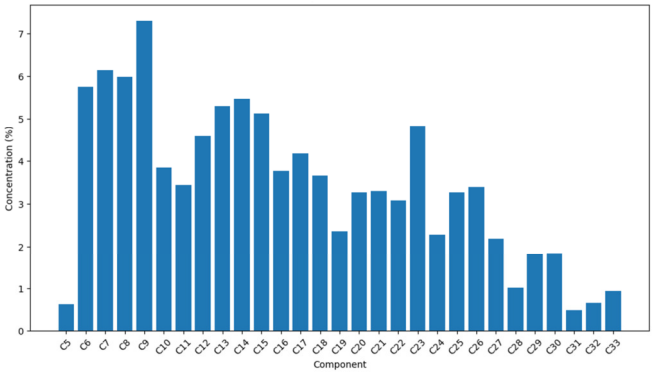

Fig. 17. Fluid composition from field A.

TABLE VII. FLUID COMPOSITION OF 3 SAMPLES FROM FIELD A

Chemical formula	Concentration (A-1), %	Concentration (A-2), %	Concentration (A-3), %
C_5H_{12}	0.852	0	1.092
C_6H_{14}	5.998	5.167	6.768
C_7H_{16}	7.152	4.595	7.409
C_8H_{18}	5.461	7.045	6.130
C_9H_{20}	6.706	8.076	7.964
$C_{10}H_{22}$	3.677	3.990	4.314
$C_{11}H_{24}$	3.152	3.796	3.777
$C_{12}H_{26}$	4.840	4.786	4.640
$C_{13}H_{28}$	4.316	8.296	3.910
$C_{14}H_{30}$	9.060	4.265	3.731
$C_{15}H_{32}$	4.631	4.334	7.006
$C_{16}H_{34}$	4.188	4.141	3.414
$C_{17}H_{36}$	4.470	4.705	3.827
$C_{18}H_{38}$	3.845	4.003	3.557
$C_{19}H_{40}$	0	3.757	3.591
$C_{20}H_{42}$	4.369	3.217	2.594
$C_{21}H_{44}$	4.012	3.677	2.577
$C_{22}H_{46}$	3.993	3.329	2.265
$C_{23}H_{48}$	7.383	4.340	3.344
$C_{24}H_{50}$	1.707	3.099	2.322
$C_{25}H_{52}$	3.528	3.229	3.412
$C_{26}H_{54}$	3.546	3.538	3.483
$C_{27}H_{56}$	2.470	2.579	1.786
$C_{28}H_{58}$	1.833	0.781	0.564
$C_{29}H_{60}$	0.644	1.255	3.795
$C_{30}H_{62}$	0.963	3.632	1.171
$C_{31}H_{64}$	0.534	0.548	0.426
$C_{32}H_{66}$	0.865	0.939	0.248
$C_{33}H_{68}$	0.805	0.179	0.885

TABLE VIII. FLUID COMPOSITION FOR CRUDE OIL FROM FIELD B

Chemical formula	Molecular weight, g/mol	Avg. concentration, %
C_5H_{12}	72.15	2.260
C_6H_{14}	86.17	2.904
C_7H_{16}	100.2	4.008
C_8H_{18}	114.22	9.693
C_9H_{20}	128.25	3.534
$C_{10}H_{22}$	142.28	3.778
$C_{11}H_{24}$	156.3	4.196
$C_{12}H_{26}$	170.33	3.884
$C_{13}H_{28}$	184.35	4.709
$C_{14}H_{30}$	198.38	4.364
$C_{15}H_{32}$	212.41	5.625
$C_{16}H_{34}$	226.43	3.818
$C_{17}H_{36}$	240.46	5.103
$C_{18}H_{38}$	254.48	3.846
$C_{19}H_{40}$	268.51	3.799
$C_{20}H_{42}$	282.54	3.306
$C_{21}H_{44}$	296.56	3.290
$C_{22}H_{46}$	310.59	2.954
$C_{23}H_{48}$	324.61	3.210
$C_{24}H_{50}$	338.64	2.632
$C_{25}H_{52}$	352.67	2.728
$C_{26}H_{54}$	366.69	2.227
$C_{27}H_{56}$	380.72	2.115
$C_{28}H_{58}$	394.74	1.658
$C_{29}H_{60}$	408.77	1.728
$C_{30}H_{62}$	422.8	1.640
$C_{31}H_{64}$	436.82	1.496
$C_{32}H_{66}$	450.85	2.106
$C_{33}H_{68}$	464.87	1.068
$C_{34}H_{70}$	478.9	1.116
$C_{35}H_{72}$	492.93	1.206

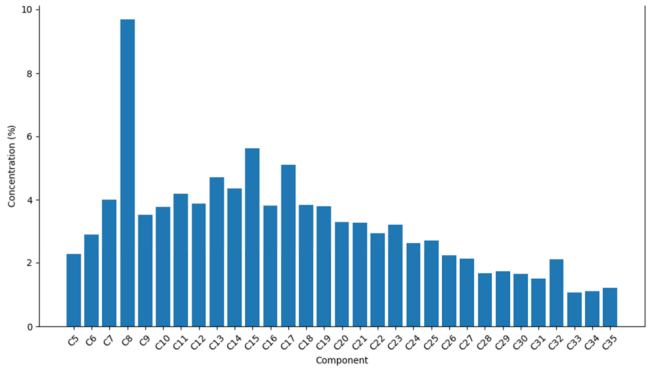

Fig. 18. Figure 16. Fluid composition from field B.

TABLE IX. FLUID COMPOSITION OF 3 SAMPLES FROM FIELD B

Chemical formula	Concentration (B-1), %	Concentration (B-2), %	Concentration (B-3), %
C_5H_{12}	2.074	1.554	3.153
C_6H_{14}	3.181	2.331	3.199
C_7H_{16}	3.913	2.885	5.227
C_8H_{18}	11.300	8.903	8.877
C_9H_{20}	3.795	3.093	3.714
$C_{10}H_{22}$	4.091	3.327	3.917
$C_{11}H_{24}$	4.488	3.795	4.307
$C_{12}H_{26}$	4.042	3.739	3.870
$C_{13}H_{28}$	4.752	4.914	4.459
$C_{14}H_{30}$	4.764	3.951	4.375
$C_{15}H_{32}$	6.086	4.505	6.284
$C_{16}H_{34}$	3.767	3.897	3.791
$C_{17}H_{36}$	5.405	4.889	5.014
$C_{18}H_{38}$	4.357	3.273	3.909
$C_{19}H_{40}$	4.155	3.921	3.320

$C_{20}H_{42}$	3.335	3.679	2.903
$C_{21}H_{44}$	3.253	3.713	2.903
$C_{22}H_{46}$	2.900	3.248	2.714
$C_{23}H_{48}$	3.035	3.698	2.898
$C_{24}H_{50}$	2.428	2.948	2.520
$C_{25}H_{52}$	2.450	3.057	2.677
$C_{26}H_{54}$	1.884	2.536	2.260
$C_{27}H_{56}$	1.666	2.507	2.172
$C_{28}H_{58}$	1.258	2.048	1.666
$C_{29}H_{60}$	1.303	2.223	1.658
$C_{30}H_{62}$	1.280	2.111	1.529
$C_{31}H_{64}$	0.961	1.630	1.897
$C_{32}H_{66}$	1.240	2.958	2.119
$C_{33}H_{68}$	1.361	1.163	0.679
$C_{34}H_{70}$	0.836	1.907	0.606
$C_{35}H_{72}$	0.640	1.596	1.382

TABLE X. FLUID COMPOSITION FOR CRUDE OIL FROM FIELD C

Chemical formula	Molecular weight, g/mol	Avg. concentration, %
C_5H_{12}	72.15	0.679
C_6H_{14}	86.17	1.351
C_7H_{16}	100.2	2.613
C_8H_{18}	114.22	5.167
C_9H_{20}	128.25	6.018
$C_{10}H_{22}$	142.28	6.817
$C_{11}H_{24}$	156.3	4.457
$C_{12}H_{26}$	170.33	4.184
$C_{13}H_{28}$	184.35	3.463
$C_{14}H_{30}$	198.38	2.647
$C_{15}H_{32}$	212.41	2.444
$C_{16}H_{34}$	226.43	2.465
$C_{17}H_{36}$	240.46	2.416
$C_{18}H_{38}$	254.48	5.488
$C_{19}H_{40}$	268.51	2.603
$C_{20}H_{42}$	282.54	2.641
$C_{21}H_{44}$	296.56	3.684
$C_{22}H_{46}$	310.59	3.494
$C_{23}H_{48}$	324.61	3.331
$C_{24}H_{50}$	338.64	3.166
$C_{25}H_{52}$	352.67	5.183
$C_{26}H_{54}$	366.69	5.029
$C_{27}H_{56}$	380.72	3.798
$C_{28}H_{58}$	394.74	3.283
$C_{29}H_{60}$	408.77	3.060
$C_{30}H_{62}$	422.8	2.502
$C_{31}H_{64}$	436.82	2.851
$C_{32}H_{66}$	450.85	2.016
$C_{33}H_{68}$	464.87	1.581
$C_{34}H_{70}$	478.9	1.570

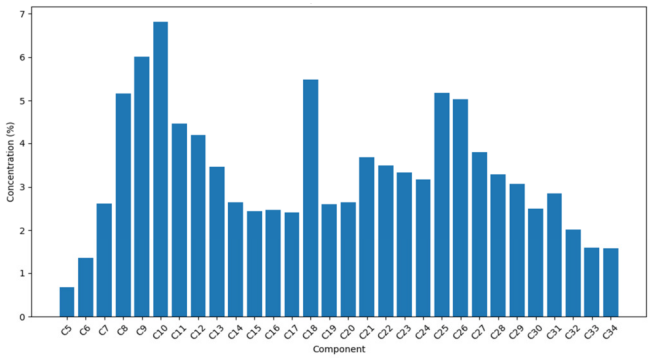

Fig. 19. Fluid composition from field C.

TABLE XI. FLUID COMPOSITION OF 3 SAMPLES FROM FIELD C

Chemical formula	Concentration (C-1), %	Concentration (C-2), %	Concentration (C-3), %
C_5H_{12}	1.268	0.491	0.278
C_6H_{14}	1.439	1.213	1.401
C_7H_{16}	3.548	2.156	2.135
C_8H_{18}	3.255	6.683	5.562
C_9H_{20}	5.788	6.401	5.864
$C_{10}H_{22}$	5.65	7.257	7.544
$C_{11}H_{24}$	6.477	3.398	3.496
$C_{12}H_{26}$	4.509	3.791	4.252
$C_{13}H_{28}$	4.274	2.83	3.284
$C_{14}H_{30}$	3.747	2.536	1.657
$C_{15}H_{32}$	2.565	2.307	2.461
$C_{16}H_{34}$	2.399	2.31	2.686
$C_{17}H_{36}$	2.362	2.337	2.55
$C_{18}H_{38}$	5.949	5.352	5.164
$C_{19}H_{40}$	2.988	2.4	2.421
$C_{20}H_{42}$	2.058	2.372	3.493
$C_{21}H_{44}$	2.257	4.13	4.667
$C_{22}H_{46}$	3.505	3.632	3.345
$C_{23}H_{48}$	3.615	3.238	3.14
$C_{24}H_{50}$	3.613	3.173	2.712
$C_{25}H_{52}$	6.061	4.971	4.517
$C_{26}H_{54}$	4.852	4.677	5.556
$C_{27}H_{56}$	3.003	4.272	4.118
$C_{28}H_{58}$	2.198	4.014	3.638
$C_{29}H_{60}$	2.662	3.189	3.328
$C_{30}H_{62}$	3.097	1.976	2.432
$C_{31}H_{64}$	2.747	2.622	3.185
$C_{32}H_{66}$	1.569	2.521	1.958
$C_{33}H_{68}$	1.2	2	1.544
$C_{34}H_{70}$	1.346	1.751	1.612

TABLE XII. FLUID COMPOSITION FOR CRUDE OIL FROM FIELD D

Chemical formula	Molecular weight, g/mol	Avg. concentration, %
C_5H_{12}	72.15	1.573
C_6H_{14}	86.17	1.868
C_7H_{16}	100.2	4.808
C_8H_{18}	114.22	9.931
C_9H_{20}	128.25	3.485
$C_{10}H_{22}$	142.28	7.763
$C_{11}H_{24}$	156.3	3.625
$C_{12}H_{26}$	170.33	4.415
$C_{13}H_{28}$	184.35	4.004
$C_{14}H_{30}$	198.38	4.070
$C_{15}H_{32}$	212.41	4.073
$C_{16}H_{34}$	226.43	4.139
$C_{17}H_{36}$	240.46	3.744
$C_{18}H_{38}$	254.48	3.966
$C_{19}H_{40}$	268.51	3.496
$C_{20}H_{42}$	282.54	4.449
$C_{21}H_{44}$	296.56	3.140
$C_{22}H_{46}$	310.59	4.328
$C_{23}H_{48}$	324.61	3.207
$C_{24}H_{50}$	338.64	2.487
$C_{25}H_{52}$	352.67	1.813
$C_{26}H_{54}$	366.69	0.564
$C_{27}H_{56}$	380.72	1.720
$C_{28}H_{58}$	394.74	1.609
$C_{29}H_{60}$	408.77	1.838
$C_{30}H_{62}$	422.8	2.907
$C_{31}H_{64}$	436.82	1.333
$C_{32}H_{66}$	450.85	1.594

$C_{33}H_{68}$	464.87	1.377
$C_{34}H_{70}$	478.9	1.454
$C_{35}H_{72}$	492.93	1.217

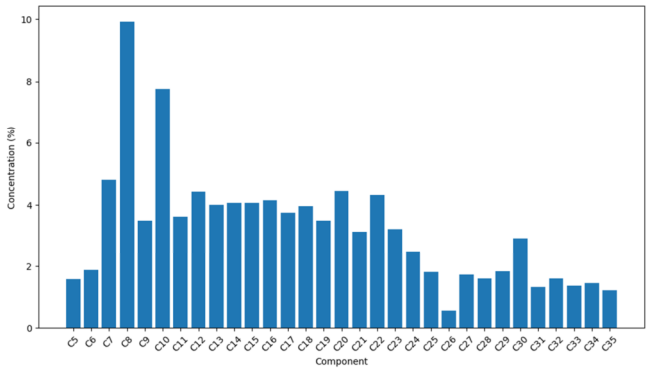

Fig. 20. Fluid composition from field D.

TABLE XIII. FLUID COMPOSITION OF 3 SAMPLES FROM FIELD D

Chemical formula	Concentration (D-1), %	Concentration (D-2), %	Concentration (D-3), %
C_5H_{12}	1.223	1.932	1.565
C_6H_{14}	1.903	2.169	1.532
C_7H_{16}	2.78	5.547	6.098
C_8H_{18}	8.995	10.284	10.515
C_9H_{20}	4.15	3.089	3.217
$C_{10}H_{22}$	10.195	6.230	6.862
$C_{11}H_{24}$	4.397	3.360	3.118
$C_{12}H_{26}$	4.74	4.050	4.455
$C_{13}H_{28}$	3.728	3.581	4.704
$C_{14}H_{30}$	5.065	3.259	3.887
$C_{15}H_{32}$	3.904	4.590	3.726
$C_{16}H_{34}$	4.235	4.322	3.861
$C_{17}H_{36}$	4.104	3.897	3.231
$C_{18}H_{38}$	4.497	3.753	3.649
$C_{19}H_{40}$	3.303	3.918	3.265
$C_{20}H_{42}$	3.645	4.668	5.035
$C_{21}H_{44}$	2.766	3.009	3.646
$C_{22}H_{46}$	3.708	4.913	4.362
$C_{23}H_{48}$	1.225	4.314	4.083
$C_{24}H_{50}$	2.969	2.310	2.182
$C_{25}H_{52}$	1.512	2.280	1.648
$C_{26}H_{54}$	1.392	0.029	0.271
$C_{27}H_{56}$	1.744	1.911	1.506
$C_{28}H_{58}$	2.314	1.818	0.695
$C_{29}H_{60}$	1.155	2.493	1.865
$C_{30}H_{62}$	3.548	2.154	3.018
$C_{31}H_{64}$	1.692	0.923	1.384
$C_{32}H_{66}$	1.128	1.495	2.161
$C_{33}H_{68}$	1.219	1.404	1.508
$C_{34}H_{70}$	1.758	0.976	1.629
$C_{35}H_{72}$	1.01	1.320	1.320

TABLE XIV. FLUID COMPOSITION FOR CRUDE OIL FROM FIELD E

Chemical formula	Molecular weight, g/mol	Avg. concentration, %
C_5H_{12}	72.15	2.513
C_6H_{14}	86.17	1.778
C_7H_{16}	100.2	10.555
C_8H_{18}	114.22	6.921
C_9H_{20}	128.25	8.931
$C_{10}H_{22}$	142.28	9.327
$C_{11}H_{24}$	156.3	4.146
$C_{12}H_{26}$	170.33	4.994
$C_{13}H_{28}$	184.35	4.262
$C_{14}H_{30}$	198.38	3.798
$C_{15}H_{32}$	212.41	4.890
$C_{16}H_{34}$	226.43	3.486
$C_{17}H_{36}$	240.46	3.555
$C_{18}H_{38}$	254.48	3.961
$C_{19}H_{40}$	268.51	3.506
$C_{20}H_{42}$	282.54	3.468
$C_{21}H_{44}$	296.56	2.788
$C_{22}H_{46}$	310.59	2.694
$C_{23}H_{48}$	324.61	2.663
$C_{24}H_{50}$	338.64	3.241
$C_{25}H_{52}$	352.67	2.337
$C_{26}H_{54}$	366.69	3.108
$C_{27}H_{56}$	380.72	3.078

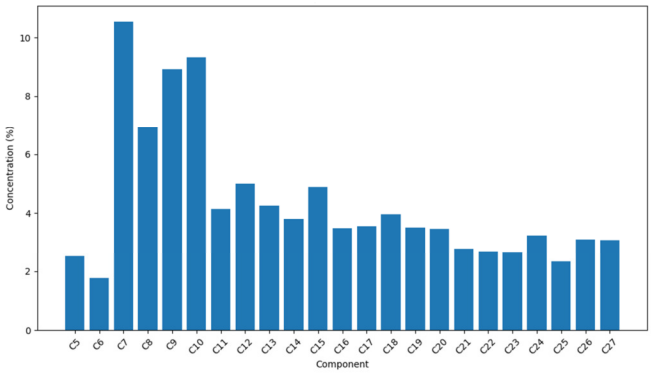

Fig. 21. Fluid composition from field E.

TABLE XV. FLUID COMPOSITION OF 3 SAMPLES FROM FIELD E

Chemical formula	Concentration (E-1), %	Concentration (E-2), %	Concentration (E-3), %
C_5H_{12}	2.55	2.606	2.383
C_6H_{14}	1.752	1.703	1.88
C_7H_{16}	9.32	10.99	11.354
C_8H_{18}	6.745	7.065	6.954
C_9H_{20}	8.742	8.573	9.477
$C_{10}H_{22}$	8.972	9.355	9.653
$C_{11}H_{24}$	3.827	4.305	4.305
$C_{12}H_{26}$	5.377	4.486	5.117
$C_{13}H_{28}$	4.115	4.133	4.537
$C_{14}H_{30}$	3.828	3.626	3.94
$C_{15}H_{32}$	7.79	3.551	3.33
$C_{16}H_{34}$	3.271	3.481	3.704
$C_{17}H_{36}$	3.819	3.511	3.334
$C_{18}H_{38}$	3.915	4.166	3.802
$C_{19}H_{40}$	3.536	3.436	3.547
$C_{20}H_{42}$	3.11	4.099	3.195
$C_{21}H_{44}$	2.69	2.986	2.688
$C_{22}H_{46}$	2.992	1.878	3.212
$C_{23}H_{48}$	2.845	2.887	2.256
$C_{24}H_{50}$	3.138	3.495	3.091
$C_{25}H_{52}$	2.413	2.457	2.143
$C_{26}H_{54}$	2.859	3.122	3.343
$C_{27}H_{56}$	2.393	4.088	2.754

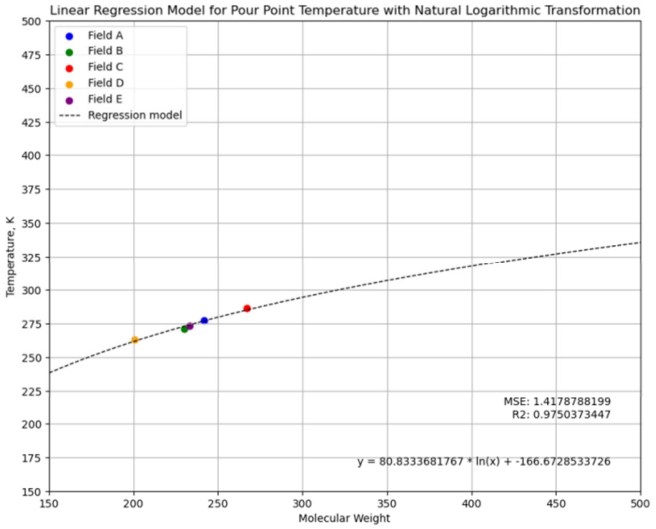

Fig. 22. Linear regression model for pour point temperature with natural logarithmic transformation.

C. Correlation Modification

This section delineates the methodological and analytical procedures undertaken to preprocess and explore laboratory experimental data, with the aim of constructing a robust linear regression model. The dataset encompasses measurements of mixture compositions alongside corresponding melting and pour points temperatures, gleaned from five distinct laboratory experiment sets. The overarching objective is to delineate a predictive model elucidating the nuanced relationship between the molecular weight of the mixture and the observed temperatures [27]. Experimental data, housed in Excel files, were systematically ingested into the Python environment. Each Excel file, corresponding to a unique laboratory experiment, comprised three distinct sheets, each harboring essential data points.

After our linear regression analysis, we have derived new equations that reflect the complex relationships between the variables under study. These equations serve as an accurate tool for determining the formation of paraffins inherent in Kazakh deposits.

Modified formula for Melting Point:

$$T_w = 71.4152111390 * ln(MW_i) - 109.3111576707 \quad (33)$$

Original formula for Melting Point [3]:

$$T_w = 374.5 + 0.02617 \times MW_i - \frac{20172}{MW_i} \quad (34)$$

Modified formula for SS point:

$$T_n = 80.8333681767 * ln(MW_i) - 166.6728533726 \quad (35)$$

Original formula for SS point [6]:

$$T_n = 366.39775 + 0.03609 \times MW_i - \frac{2.08796 \times 10^4}{MW_i} \quad (36)$$

It can be concluded (Figure 23) that the new correlation gives much closer melting point values for compounds with different molecular weight, while the original formula gives a noticeable uncertainty for some of the compounds with lower molecular weights compared to the reference data [28].

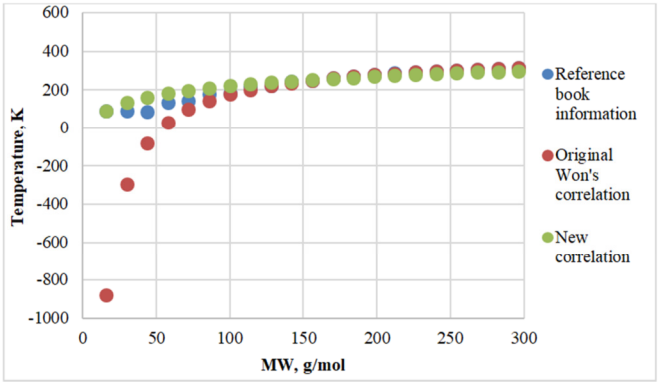

Fig. 23. Correlation comparison.

IV. CONCLUSION

This study investigated the fusion properties of Kazakhstani crude oil, specifically the melting point and solid-state transition temperatures, using five distinct oil samples. Data on the compositional makeup of the crude oil were obtained through gas chromatography, while the fusion properties were determined using advanced analytical equipment, including Differential Scanning Calorimeter and Pour Point Testing. Based on the experimental data, novel correlations were developed using linear and logarithmic regression techniques. These correlations demonstrated superior accuracy for the Kazakhstani crude oil compared to the widely used models of [3] and [6], which have traditionally formed the basis for wax precipitation predictions in prior studies.

The accuracy of the proposed correlations was validated through comparative analysis of melting point data for various hydrocarbon compounds with differing molecular weights. The results, supported by graphical comparisons with reference data, illustrate the significant improvements offered by the new model over existing approaches.

This research underscores the necessity of developing predictive models tailored to the unique compositional characteristics of regional crude oils. It highlights the limitations of generalized approaches, advocating for models that account for specific field conditions. Future studies could extend this methodology to other crude oil fields, incorporate additional parameters such as pressure and chemical additives, and explore the effects of environmental variables on wax precipitation behavior. These advancements would contribute to the development of more precise and adaptable predictive tools for flow assurance in the petroleum industry.

This work not only provides valuable insights into the properties of Kazakhstani crude oil but also establishes a

framework for refining wax precipitation models that can be applied globally to address similar challenges in cold climate operations.

ACKNOWLEDGMENTS

This research was carried out with the financial support of the Science Committee of the Ministry of Science and Higher Education of the Republic of Kazakhstan (BR21881822 Development of technological solutions for optimizing geological and technical operations when drilling wells and oil production at the late stage of field exploitation, 2023–2025).

REFERENCES

[1] J. H. Hansen, Aa. Fredenslund, K. S. Pedersen, and H. P. Rønningsen, "A thermodynamic model for predicting wax formation in crude oils," *AIChE Journal*, vol. 34, no. 12, pp. 1937–1942, 1988, https://doi.org/10.1002/aic.690341202.

[2] R. Venkatesan, N. R. Nagarajan, K. Paso, Y.-B. Yi, A. M. Sastry, and H. S. Fogler, "The strength of paraffin gels formed under static and flow conditions," *Chemical Engineering Science*, vol. 60, no. 13, pp. 3587–3598, Jul. 2005, https://doi.org/10.1016/j.ces.2005.02.045.

[3] K. W. Won, "Thermodynamics for solid solution-liquid-vapor equilibria: wax phase formation from heavy hydrocarbon mixtures," *Fluid Phase Equilibria*, vol. 30, pp. 265–279, Jan. 1986, https://doi.org/10.1016/0378-3812(86)80061-9.

[4] K. W. Won, "Thermodynamic calculation of cloud point temperatures and wax phase compositions of refined hydrocarbon mixtures," *Fluid Phase Equilibria*, vol. 53, pp. 377–396, Dec. 1989, https://doi.org/10.1016/0378-3812(89)80104-9.

[5] Z. Baishemirov, J.-G. Tang, K. Imomnazarov, and M. Mamatqulov, "Solving the problem of two viscous incompressible fluid media in the case of constant phase saturations," *Open Engineering*, vol. 6, pp. 742–745, Dec. 2016, https://doi.org/10.1515/eng-2016-0100.

[6] D. V. Nichita, L. Goual, and A. Firoozabadi, "Wax Precipitation in Gas Condensate Mixtures," *SPE Production & Facilities*, vol. 16, no. 4, pp. 250–259, Nov. 2001, https://doi.org/10.2118/74686-PA.

[7] H. Pan, A. Firoozabadi, and P. Fotland, "Pressure and Composition Effect on Wax Precipitation: Experimental Data and Model Results," *SPE Production & Facilities*, vol. 12, no. 4, pp. 250–258, Nov. 1997, https://doi.org/10.2118/36740-PA.

[8] J. Xue, C. Li, and Q. He, "Modeling of wax and asphaltene precipitation in crude oils using four-phase equilibrium," *Fluid Phase Equilibria*, vol. 497, pp. 122–132, Oct. 2019, https://doi.org/10.1016/j.fluid.2019.06.011.

[9] C. Lira-Galeana, A. Firoozabadi, and J. M. Prausnitz, "Thermodynamics of wax precipitation in petroleum mixtures," *AIChE Journal*, vol. 42, no. 1, pp. 239–248, 1996, https://doi.org/10.1002/aic.690420120.

[10] K. Schou Pedersen, P. Skovborg, and H. P. Roenningsen, "Wax precipitation from North Sea crude oils. 4. Thermodynamic modeling," *Energy & Fuels*, vol. 5, no. 6, pp. 924–932, Nov. 1991, https://doi.org/10.1021/ef00030a022.

[11] M. R. Riazi, *Characterization and Properties of Petroleum Fractions*. West Conshohocken, PA, USA: ASTM International, 2005.

[12] J. A. P. Coutinho, "Predictive UNIQUAC: A New Model for the Description of Multiphase Solid−Liquid Equilibria in Complex Hydrocarbon Mixtures," *Industrial & Engineering Chemistry Research*, vol. 37, no. 12, pp. 4870–4875, Dec. 1998, https://doi.org/10.1021/ie980340h.

[13] J. A. P. Coutinho, B. Edmonds, T. Moorwood, R. Szczepanski, and X. Zhang, "Reliable Wax Predictions for Flow Assurance," *Energy & Fuels*, vol. 20, no. 3, pp. 1081–1088, May 2006, https://doi.org/10.1021/ef050082i.

[14] W. Chen, Z. Zhao, X. Zhang, and L. Wang, "Thermodynamic phase equilibria of wax precipitation in crude oils," *Fluid Phase Equilibria*, vol. 255, no. 1, pp. 31–36, Jul. 2007, https://doi.org/10.1016/j.fluid.2007.03.015.

[15] J. Yang, W. Wang, B. Shi, Q. Ma, P. Song, and J. Gong, "Prediction of wax precipitation with new modified regular solution model," *Fluid Phase Equilibria*, vol. 423, pp. 128–137, Sep. 2016, https://doi.org/10.1016/j.fluid.2016.04.015.

[16] J. C. M. Escobar-Remolina, "Prediction of characteristics of wax precipitation in synthetic mixtures and fluids of petroleum: A new model," *Fluid Phase Equilibria*, vol. 240, no. 2, pp. 197–203, Feb. 2006, https://doi.org/10.1016/j.fluid.2005.12.033.

[17] R. Dalirsefat and F. Feyzi, "A thermodynamic model for wax deposition phenomena," *Fuel*, vol. 86, no. 10, pp. 1402–1408, Jul. 2007, https://doi.org/10.1016/j.fuel.2006.11.034.

[18] A. R. S. Nazar, B. Dabir, and M. R. Islam, "A Multi-Solid Phase Thermodynamic Model for Predicting Wax Precipitation in Petroleum Mixtures," *Energy Sources*, vol. 27, no. 1–2, pp. 173–184, Jan. 2005, https://doi.org/10.1080/00908310490448253.

[19] E. Ghanaei, F. Esmaeilzadeh, and J. F. Kaljahi, "New Multi-Solid Thermodynamic Model for the Prediction of Wax Formation," *International Journal of Chemical and Molecular Engineering*, vol. 1, no. 5, pp. 48–53, 2007.

[20] C. Ghotbi, M. H. Mashhadi, and B. T. Jafari, "Thermodynamic modeling of wax precipitation in crude oil based on PC-saft model," in *12th International Conference on Heat Transfer, Fluid Mechanics and Thermodynamics*, Malaga, Spain, Jul. 2016, pp. 1058–1067.

[21] M. Mansourpoor, R. Azin, S. Osfouri, and A. A. Izadpanah, "Study of wax disappearance temperature using multi-solid thermodynamic model," *Journal of Petroleum Exploration and Production Technology*, vol. 9, no. 1, pp. 437–448, Mar. 2019, https://doi.org/10.1007/s13202-018-0480-1.

[22] E. D. Ivanchina, E. N. Ivashkina, G. Yu. Nazarova, and G. Zh. Seitenova, "Influence of Feedstock Group Composition on the Octane Number and Composition of the Gasoline Fraction of Catalytically Cracked Vacuum Distillate," *Petroleum Chemistry*, vol. 58, no. 3, pp. 225–236, Mar. 2018, https://doi.org/10.1134/S0965544118030106.

[23] L. Tugashova, R. Bazhenov, U. Abdyldaeva, I. Korosteleva, and E. Muromtseva, "A simulation modeling approach used in the crude oil refining process," *Journal of Physics: Conference Series*, vol. 2373, no. 6, Dec. 2022, Art. no. 062003, https://doi.org/10.1088/1742-6596/2373/6/062003.

[24] E. Krivosheev and R. Sayakhov. *Gas chromatography. Guidelines for laboratory work: Method*, Kazan National Research Technological University, 2020

[25] S. Rehman, "Machine Learning Guide for Petroleum Professionals: Part 1," *TWA*, Feb. 07, 2023. https://jpt.spe.org/twa/a-machine-learning-guide-for-petroleum-professionals-part-1.

[26] W. B. Kay, "Density of Hydrocarbon Gases and Vapors at High Temperature and Pressure," *Industrial & Engineering Chemistry Research*, vol. 28, no. 9, pp. 1014–1019, 1936.

[27] E. V. Asbaghi and M. Assareh, "Application of a sequential multi-solid-liquid equilibrium approach using PC-SAFT for accurate estimation of wax formation," *Fuel*, vol. 284, Jan. 2021, Art. no. 119010, https://doi.org/10.1016/j.fuel.2020.119010.

[28] S. I. Eyitayo *et al.*, "A Comparative Evaluation of Selected Correlations for Estimating Wax-Appearance Temperature of Crude Oils," in *SPE Nigeria Annual International Conference and Exhibition*, Aug. 2020, pp. 1–7, https://doi.org/10.2118/203618-MS.